Chinese Chemical Letters 33 (2022) 2069–2072

Contents lists available at ScienceDirect

Chinese Chemical Letters

journal homepage: www.elsevier.com/locate/cclet

NiCu bimetallic catalysts derived from layered double hydroxides for hydroconversion of *n*-heptane

Yanru Zhu, Minghuan Yang, Zhen Zhang, Zhe An, Jian Zhang, Xin Shu, Jing He*

State Key Laboratory of Chemical Resource Engineering, Beijing Advanced Innovation Center for Soft Matter Science and Engineering, Beijing University of Chemical Technology, Beijing 100029, China

ARTICLE INFO

Article history:
Received 9 May 2021
Revised 29 July 2021
Accepted 29 August 2021
Available online 4 September 2021

Keywords:
n-Heptane reforming
NiCu bimetallic catalysts
Synergic catalysis
Uniform distribution
Layered double hydroxides

ABSTRACT

Supported NiCu bimetallic catalysts have been produced *in-situ* on commercial Al_2O_3 by using layered double hydroxides as precursors. The resulting catalysts show a uniform Ni and Cu distribution, thus providing good activity and selectivity in the reforming reaction of *n*-heptane. The catalytic performance has been found to depend on the Cu/Ni ratio, revealing the synergic catalysis between homogeneously dispersed Ni and Cu sites. The good catalysis of NiCu bimetallic catalysts makes it possible to partly or even completely replace Pt with NiCu bimetallic catalysts.

Supported Pt is a common catalyst for the catalytic reforming reaction [1–4]. Considerable efforts have recently been dedicated to the development of low-cost and highly efficient non-platinum reforming catalysts, and great progress has been made with tungsten carbide [5], Mo-based catalysts such as Mo_2C [6], MoO_xC_y [7] and MoO_x [8–10], as well as supported Ni [11–13] and Co [13] catalysts. The great challenges with non-platinum reforming catalysts originate from substantial hydrogenolysis and cracking reactions [14], which result in low isomerization selectivity. Increasing the dispersion of supported metals has been found to contribute to isomerization selectivity [15]. For example, Ni-La/HY catalyst exhibits higher isomerization selectivity than Ni/HY in the hydroconversion of *n*-C_8 because the metal dispersion has been improved by rare earth addition [15]. Yet the reforming performance of non-noble metal catalyst has not been reported to reach that of Pt catalyst. The bimetallic catalyst, in which small amount of platinum is used together with non-noble metal components such as Ni [16,17] or Cu [18], is till now a good choice to obtain good activity and selectivity while reduce the cost of catalysts. For example, with proper Pt proportions, the Ni-Pt bimetallic catalysts afford higher activity and are more selective to di-branched alkanes than Pt monometallic catalyst in the hydroconversion of *n*-C_6 reaction [17]. The complete replacement of platinum with transition metals in the paraffin reforming process remains a great challenge.

In this work, the feasibility to partly or even completely replace Pt with NiCu bimetallic catalyst has been demonstrated, with Ni and Cu in a highly homogeneous dispersion by using Ni and Cu containing layered double hydroxides as precursors. Layered double hydroxides (LDHs), a hydrotalcite-like compound, have been demonstrated to be excellent precursors for supported metal catalysts [19–23]. This work reports the homogeneously dispersed Ni and Cu centers, which affords good activity and selectivity in the reforming reaction of *n*-heptane. The NiCu bimetallic catalyst even provides higher activity than Pt catalyst while with comparable selectivity.

The Ni and Cu containing ZnAl-LDHs precursors were prepared *in situ* on γ-Al_2O_3 support according to the reported method [24]. The Cu/Ni molar ratios were controlled as 0.61, 1.19, 2.11 and 3.17 as determined by inductively coupled plasma optic emission spectrometer (ICP-OES) analysis (Table S1 in Supporting information). The Ni and Cu containing ZnAl-LDHs precursors were activated in the reactor by first calcining in the air at 550 °C and then reducing with H_2 flow at 500 °C. The resulting sample was denoted $NiCu_x$-ZnAl-LDO@Al_2O_3 (x represents the Cu/Ni molar ratio). The reaction was initiated by introducing *n*-C_7 into the reactor, and the products were analysed on-line with a gas chromatograph. For comparison, the supported NiCu bimetallic catalyst with a Cu/Ni molar ratio of 1.14 was also prepared by incipient wetness impregnation method (denoted $NiCu_{1.14}$/ZnAl-LDO@Al_2O_3), followed by the same calcination and reduction process as for $NiCu_x$-ZnAl-LDO@Al_2O_3.

The powder X-ray diffraction (XRD) patterns pattern for each $NiCu_x$-ZnAl-LDHs@Al_2O_3 sample (Fig. 1A and Fig. S1 in Supporting

* Corresponding author.
E-mail addresses: jinghe@263.net.cn, hejing@mail.buct.edu.cn (J. He).

https://doi.org/10.1016/j.cclet.2021.08.120
1001-8417/

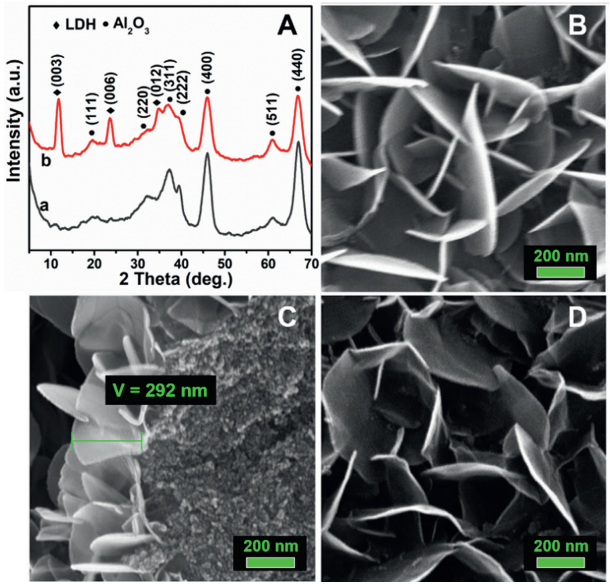

Fig. 1. (A) XRD patterns of (a) γ-Al_2O_3, (b) $NiCu_{1.19}$-ZnAl-LDHs@Al_2O_3 with a Cu/Ni molar ratio of 1.19; (B) SEM images of the surface; (C) the cross section of the $NiCu_{1.19}$-ZnAl-LDHs@Al_2O_3; and (D) SEM images of $NiCu_{1.19}$-ZnAl-LDO@Al_2O_3 obtained from $NiCu_{1.19}$-ZnAl-LDHs@Al_2O_3.

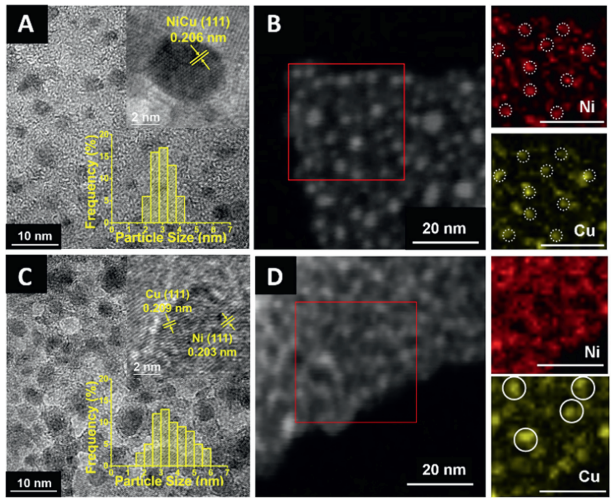

Fig. 2. TEM image (A) and HAADF-STEM image (B) of catalyst $NiCu_{1.19}$-ZnAl-LDO@Al_2O_3; TEM image (C) and HAADF-STEM image (D) of catalyst $NiCu_{1.14}$/ZnAl-LDO@Al_2O_3. Insets in (A) and (C) are the HRTEM images and the particle size frequency distribution histograms. Insets in (B) and (D) are the elemental mapping images of Ni and Cu for the corresponding sample. Scale bar: 20 nm.

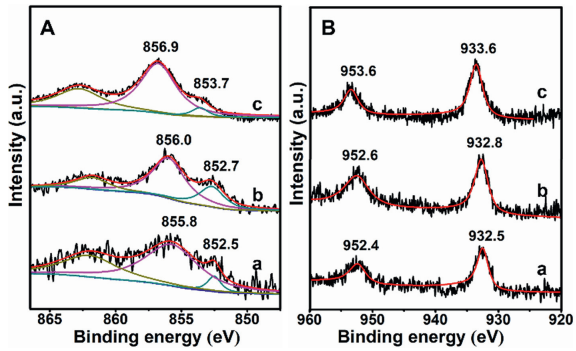

Fig. 3. Ni (A) and Cu (B) 2p XPS spectra for (a) $NiCu_{1.14}$/ZnAl-LDO@Al_2O_3, (b) $NiCu_{1.19}$-ZnAl-LDO@Al_2O_3, and (c) 0.17%Pt/ $NiCu_{1.19}$-ZnAl-LDO@Al_2O_3.

information) clearly illustrates the [003], [006] and [012] reflections characteristic of the structure of hydrotalcites [25], indicating the formation of LDHs on the γ-Al_2O_3 support. No other crystalline phases were detected in addition to γ-Al_2O_3 support and LDHs. Flake-shaped NiCuZnAl-LDHs crystallites can be observed from the SEM image (Fig. 1B) as growing in interlaced direction on the surface of Al_2O_3. As can be seen from the cross section of NiCuZnAl-LDHs@Al_2O_3 (Fig. 1C), LDHs phase grows on the Al_2O_3 surface in a thickness of about 292 nm, with the edges of LDH slabs tightly adhered to Al_2O_3 spheres. The growths of LDHs and the corresponding LDO results in the specific surface area increasing from 187 m^2/g (for γ-Al_2O_3) to 218 m^2/g (for $NiCu_{1.19}$-ZnAl-LDHs@Al_2O_3) or 212 m^2/g (for $NiCu_{1.19}$-ZnAl-LDO@Al_2O_3), probably because the LDHs or LDO crystallites raise the surface roughness. The calcination and reduction cause no visible destruction of the LDH morphology or change in surface area on Al_2O_3 surface, and the resulting $NiCu_{1.19}$-ZnAl-LDO@Al_2O_3 well retains the interlaced arrangement of flake-shaped slabs (Fig. 1D).

The transmission electron microscopy (TEM) image (Fig. 2A) shows that the metal nanoparticles are homogeneously dispersed in $NiCu_{1.19}$-ZnAl-LDO@Al_2O_3. The particles are in a narrow size distribution from 1.9 nm to 4.2 nm with the maximum of around 3.0 nm, and the lattice spacing of the exposed NiCu (111) facet is 0.206 nm in the high-resolution TEM (HRTEM) image (inset in Fig. 2A). The high angle annular dark-field scanning transmission electron microscopy (HAADF-STEM) image (Fig. 2B) indicates a uniform distribution of the metal nanoparticles, just as observed from the TEM image. The STEM-energy dispersive X-ray (EDX) elemental mapping (insets in Fig. 2B) displays that the Ni and Cu elements are distributed homogeneously and almost in the same position. The observations from HRTEM image and EDX mapping illustrate a NiCu alloy structure, which is consistent with an earlier report [26]. As a comparison, the metal particles in the $NiCu_{1.14}$/ZnAl-LDO@Al_2O_3 are diverse in morphology (Fig. 2C), with a broader size distribution from 1.7 nm to 6.0 nm, as observed in TEM image. Separated Ni and Cu particles with both (111) facet exposed are observed in HRTEM image (inset in Fig. 2C). The HAADF-STEM image provides a more obvious difference in the metal distribution between $NiCu_{1.14}$/ZnAl-LDO@Al_2O_3 and $NiCu_{1.19}$-ZnAl-LDO@Al_2O_3). The metal particles are observed to be in a continuous and more chaotic distribution in the HAADF-STEM image of $NiCu_{1.14}$/ZnAl-LDO@Al_2O_3, with visible aggregation (Fig. 2D). The EDX image (insets in Fig. 2D) exhibit a discrepant Ni and Cu element distribution. In the XPS spectra (Fig. 3), the binding energies of Ni^0 and Cu^0 [27,28] are measured as 852.7 and 932.8 eV for $NiCu_{1.19}$-ZnAl-LDO@Al_2O_3 (Fig. 3A), 0.2 and 0.3 eV higher than that for $NiCu_{1.14}$/ZnAl-LDO@Al_2O_3 (Fig. 3B), consistent with better NiCu dispersion in $NiCu_{1.19}$-ZnAl-LDO@Al_2O_3. The adjacent binding energy at 855.8-856.9 eV in the Ni $2p_{3/2}$ XPS spectra originates from a high-spin divalent state of Ni^{2+} in the sample [27]. When nickel is alloyed with copper, changes in the electronic properties of nickel result in displacement of BEs to lower values depending on the copper content.

In the hydro-conversion of heptane (n-C_7) (Table 1), $NiCu_{1.19}$-ZnAl-LDO@Al_2O_3 as the catalyst (Table 1, entry 1) shows visibly higher n-C_7 conversion, higher specific activity, higher i-C_7 selectivity, and lower C_1-C_4 selectivity than $NiCu_{1.14}$/ZnAl-LDO@Al_2O_3 (Table 1, entry 2). The n-C_7 conversion over $NiCu_{1.19}$-ZnAl-LDO@Al_2O_3 is even higher than over Pt/ZnAl-LDO@Al_2O_3 with a 0.32% Pt loading (Table 1, entry 3), while with almost the same selectivity. The better apparent activity and isomerization selectivity of $NiCu_{1.19}$-ZnAl-LDO@Al_2O_3 is supposed to owe to the well-alloyed structure with NiCu uniform distribution. As revealed by the XPS results, the *in situ* exsolution of NiCu from

Table 1
Catalytic results for the hydroconversion of n-C_7.[a]

Entry	Catalyst[b]	Conversion (%)	Specific activity (mol mol^{-1} h^{-1})[c]	Selectivity (%)		
				i-C_7	Toluene	C_1-C_4
1	$NiCu_{1.19}$-ZnAl-LDO@Al_2O_3	33.8	28.8	32.9	5.0	37.5
2	$NiCu_{1.17}$/ZnAl-LDO@Al_2O_3	24.9	20.4	24.6	4.1	40.0
3	0.32%Pt/ZnAl-LDO@Al_2O_3	22.2	536.3	35.0	5.7	36.0
4	0.15%Pt/Ni-ZnAl-LDO@Al_2O_3	44.6	2340.0	21.6	3.7	33.4
5	0.16%Pt/$NiCu_{0.61}$-ZnAl-LDO@Al_2O_3	39.7	1950.0	31.5	4.9	31.3
6	0.17%Pt/$NiCu_{1.19}$-ZnAl-LDO@Al_2O_3	42.6	1972.9	38.9	6.2	26.3
7	0.17%Pt/$NiCu_{2.11}$-ZnAl-LDO@Al_2O_3	65.7	3028.2	37.4	8.0	27.2
8	0.17%Pt/$NiCu_{3.17}$-ZnAl-LDO@Al_2O_3	85.0	3900.0	28.0	16.6	29.2
9	0.14%Pt/$Cu_{1.21\%}$-ZnAl-LDO@Al_2O_3	27.0	1504.3	39.3	6.1	31.1
10	0.16%Pt/$Cu_{3.91\%}$-ZnAl-LDO@Al_2O_3	44.4	2145.0	51.2	6.3	22.9

[a] Reaction conditions: 500 °C, 0.7 MPa, H_2/n-C_7 = 6, WHSV = 4 h^{-1}.
[b] The loadings of Ni and Cu are shown in Table S1.
[c] The specific activities representative moles of n-heptane conversion on per mol metal per hour; specific activities are normalized by moles of (Ni + Cu) for NiCu-containing samples (without Pt), and are normalized by moles of Pt for Pt-containing samples.

LDHs layers provides stronger metal-supports interactions that leads to Ni and Cu centers more electron-deficient, which well accounts for the higher activity of $NiCu_{1.19}$-ZnAl-LDO@Al_2O_3 than $NiCu_{1.14}$/ZnAl-LDO@Al_2O_3. According to previous observation [29], more highly are metal centers dispersed, more is C-C cleavage inhibited. So the better selectivity of $NiCu_{1.19}$-ZnAl-LDO@Al_2O_3 than $NiCu_{1.14}$/ZnAl-LDO@Al_2O_3 could also be well explained. The use of Pt in 0.17% loading together with $NiCu_{1.19}$ bimetallic catalyst promotes both of n-C_7 conversion and i-C_7 selectivity, while largely reduces the C_1-C_4 selectivity (Table 1, entry 6). The specific activity on 0.17%Pt/$NiCu_{1.19}$-ZnAl-LDO@Al_2O_3 is 268% higher than that on 0.32%Pt/ZnAl-LDO@Al_2O_3. The significant increase in specific activity (normalized by moles of Pt) can be attributed to the contribution of NiCu. The ICP results and TEM/STEM images show that the Pt loading makes no visible impact on components of Ni or Cu and the homogeneous distribution of NiCu elements (Table S1 and Fig. S2 in Supporting information). The NiCu particles retain narrow distribution sized from 3.8 nm to 6.3 nm. In the XPS spectra (Fig. 3), a visible increase in the BEs of Ni $2p_{3/2}$ and Cu $2p_{3/2}$ is observed with Pt loaded, illuminating the electron transfer from NiCu to Pt atoms. Therefore, the promotion of catalysis observed with 0.17%Pt/$NiCu_{1.19}$-ZnAl-LDO@Al_2O_3 could originate from the synergies of NiCu and Pt centers. Similar synergy effect of the metal active sites was previously observed for the Ir-Pt/Al_2O_3 catalyst prepared by organometallic grafting method in the ring opening reaction of methyl-cyclopentane [30].

To better understand why the reforming catalysis of Ni and Cu even better than supported Pt, the Cu/Ni molar ratios (Table S1) have been varied in this work. As shown in the XPS spectra (Fig. 4), in comparison with Ni-ZnAl-LDO@Al_2O_3, Cu introduction decreases the binding energy (BE) of Ni $2p_{3/2}$ (Fig. 4A) slightly, and meanwhile the BE of Cu^0 in $NiCu_{0.61}$-ZnAl-LDO@Al_2O_3 rises in comparison to Cu-ZnAl-LDO@Al_2O_3 (Fig. 4B), consistent with the electron transfer from Cu to Ni. With increasing Cu/Ni ratio, both of Ni^0 and Cu^0 BEs successively increases. But the reason for the increase in the BEs needs more investigations. Similar trends are observed on Pt-containing samples (Figs. 4C and D).

In the hydro-conversion of n-C_7, in comparison with Ni catalyst without Cu (Table 1, entry 4), the introduction of Cu in a Cu/Ni ratio of 0.61 decreases the n-C_7 conversion while improves the isomerization selectivity visibly (Table 1, entry 5). With the Cu/Ni ratio increasing, n-C_7 conversion, specific activity, and toluene selectivity all increase, while the isomerization selectivity shows a first increasing and then decreasing change (Table 1, entries 5-8). The dependence of catalytic activity and selectivity on the Cu/Ni ratio of NiCu bimetallic catalyst indicates the synergic catalysis between highly homogeneous Ni and Cu sites [31]. The introduction of Cu in

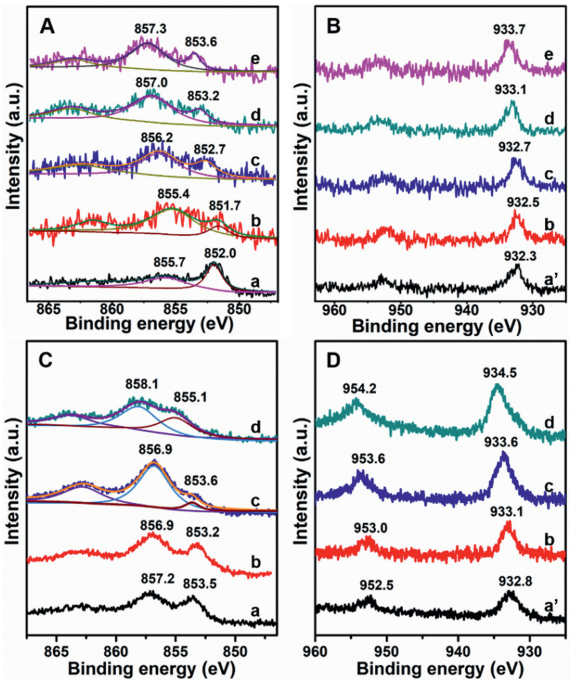

Fig. 4. Ni (A, C) and Cu (B, D) 2p XPS spectra for (a) Ni-ZnAl-LDO@Al_2O_3, (a') Cu-ZnAl-LDO@Al_2O_3, (b) $NiCu_{0.61}$-ZnAl-LDO@Al_2O_3, (c) $NiCu_{1.19}$-ZnAl-LDO@Al_2O_3, (d) $NiCu_{2.11}$-ZnAl-LDO@Al_2O_3 and (e) $NiCu_{3.17}$-ZnAl-LDO@Al_2O_3 without (A, B) and with (C, D) Pt loaded.

a Cu/Ni ratio of 0.61 increases the electronic density of Ni site, accounting for the activity reduction on Pt/$NiCu_{0.61}$-ZnAl-LDO@Al_2O_3 in comparison to Pt/Ni-ZnAl-LDO@Al_2O_3. The activity enhancement with increasing Cu/Ni ratio is well consistent with the successive decreases in the electronic density of both Cu and Ni sites.

The introduction of Cu inhibits the hydrogenolysis and/or cracking reactions, giving a reduced C_1-C_4 selectivity (Table 1, entries 4-8). But a visible inhibition of C_1-C_4 selectivity needs a higher Cu loading when no Ni is present (Table 1, entries 9 and 10). The toluene selectivity increases with Cu/Ni ratio (Table 1, entries 5-8), but not with the amount of single Cu (Table 1, entries 9 and 10), indicating the role of synergic catalysis between Cu and Ni sites in the improvement of toluene selectivity. When a small amount of Cu added, the XPS show that the binding energy of Ni shifts toward a low energy of 0.3 eV, and the binding energy of Cu increases 0.3 eV (Fig. 4). The changes of electronic structure of the metals result in a slight decrease in catalytic activity. Further in-

crease the ratio of Cu/Ni, the binding energy of Ni and Cu increases successively. The activities of catalysts show an increasing trend and the selectivity of toluene increase in sequence. The dehydrogenation ability of the metals is enhanced with the binding energy of metals increasing. The selectivity of isomerization increases at first and then decreases, while the cleavage selectivity shows an opposite trend, but the magnitude of the change is relatively small.

In the H_2-TPR profiles (Fig. S3 in Supporting information), the reduction temperature for Ni(II) gradually decreases from 596 °C to 481 °C with increasing Cu/Ni ratio, while the reduction temperature of Cu(II) decreases from 341 °C to 254 °C. Additional hydrogen consumptions are observed at 325 °C for $NiCu_{1.19}$-ZnAl-LDO@Al_2O_3 and 288 °C for $NiCu_{2.11}$-ZnAl-LDO@Al_2O_3, which suggests the possible formation of NiCu alloy phase. But the hydrogen consumption at 287 °C almost diminishes for $NiCu_{3.17}$-ZnAl-LDO@Al_2O_3.

The isomerization selectivity on 0.16%Pt/$Cu_{3.91\%}$-ZnAl-LDO@Al_2O_3 is 142% higher than on 0.15%Pt/Ni-ZnAl-LDO@Al_2O_3. The isomerization reaction rate has been reported highly dependent on the acidic property of catalysts [4]. But there is no significant difference in the amount and strength of acidic sites between 0.16%Pt/$Cu_{3.91\%}$-ZnAl-LDO@Al_2O_3 and 0.15%Pt/Ni-ZnAl-LDO@Al_2O_3, based on NH_3-TPD profiles (Fig. S4 in Supporting information). So it can be deduced that the Cu sites promote isomerization selectivity by inhibiting hydrogenolysis reaction. The synergies of Ni and Cu sites on alloy phase is mainly responsible for the higher isomerization selectivity observed with $NiCu_{1.19}$-ZnAl-LDO@Al_2O_3 and $NiCu_{2.11}$-ZnAl-LDO@Al_2O_3 than with other catalysts.

In summary, NiCu bimetallic catalyst with uniform NiCu dispersion has been demonstrated to provide higher activity than Pt catalyst while with similar selectivity in the reforming reaction of *n*-heptane. The synergies between homogeneously dispersed Ni and Cu sites account for the enhancement of activity and selectivity.

Declaration of competing interest

The authors declare no competing financial interest.

Acknowledgments

Financial supports from National Nature Science Foundation of China (NSFC, Nos. 91634120 and 21521005), the National Key Research and Development Program of China (No. 2017YFA0206804) and the Fundamental Research Funds for the Central Universities (No. XK1802-6) are gratefully acknowledged.

Supplementary materials

Supplementary material associated with this article can be found, in the online version, at doi:10.1016/j.cclet.2021.08.120.

References

[1] G.J. Antos, A.M. Aitani, Catalytic Naphtha Reforming, Revised and Expanded, second ed., CRC Press, New York, 2004.
[2] V. Haensel, U.S. Patent 2 611 736, UOP, 1952.
[3] H.E. Kluksdahl, U.S. Patent 3 415 737, UOP, 1968.
[4] N. Parsafard, M.H. Peyrovi, N. Parsafard, Chin. Chem. Lett. 28 (2017) 546–552.
[5] Á. Morales-García, F. Calle-Vallejo, F. Illas, ACS Catal. 10 (2020) 13487–13503.
[6] J.G. Chen, B. Fruhberger, J. Eng Jr., et al., J. Mol. Catal. A: Chem. 131 (1998) 285–299.
[7] A.P.E. York, C. Pham-Huu, P.D. Gallo, M.J. Ledoux, Catal. Today 35 (1997) 51–57.
[8] L.O. Alemán-Vázquez, F. Hernández-Pérez, J.L. Cano-Domínguez, et al., Fuel 117 (2014) 463–469.
[9] H. Al-Kandari, S. Al-Kandari, F. Al-Kharafi, A. Katrib, Energy Fuels 23 (2009) 5737–5742.
[10] H. Al-Kandari, F. Al-Kharafi, A. Katrib, Appl. Catal. A 383 (2010) 141–148.
[11] J. Kim, S.W. Han, J.C. Kim, et al., ACS Catal. 8 (2018) 10545–10554.
[12] P. Lanzafame, S. Perathoner, G. Centi, et al., ChemCatChem 9 (2017) 1632–1640.
[13] A. Corma, A. Martinez, S. Pergher, et al., Appl. Catal. A 152 (1997) 107–125.
[14] Y. Tan, W. Hu, Y. Du, et al., Appl. Catal. A 611 (2021) 117916.
[15] D. Li, F. Li, J. Ren, Y. Sun, Appl. Catal. A 241 (2003) 15–24.
[16] I. Eswaramoorthi, N. Lingappan, Appl. Catal. A 245 (2003) 119–135.
[17] M.H. Jordão, V. Simões, D. Cardoso, Appl. Catal. A 319 (2007) 1–6.
[18] S. Velduthi, C.H. Shin, O.S. Joo, K.D. Jung, Catal. Today 185 (2012) 88–93.
[19] M. Laipan, J. Yu, R. Zhu, et al., Mater. Horiz. 7 (2020) 715–745.
[20] Y. Zhu, H. Guo, J. Zhang, et al., Ind. Eng. Chem. Res. 59 (2020) 8649–8660.
[21] Y. Zhu, J. Zhang, X. Ma, et al., J. Catal. 389 (2020) 78–86.
[22] G. Fan, F. Li, D.G. Evans, et al., Chem. Soc. Rev. 43 (2014) 7040–7066.
[23] Y. Cao, H. Zhang, S. Ji, et al., Angew. Chem. Int. Ed. 59 (2020) 11647–11652.
[24] Y. Zhu, W. Zhao, J. Zhang, et al., ACS Catal. 10 (2020) 8032–8041.
[25] Y. Zhu, Z. An, J. He, J. Catal. 341 (2016) 44–54.
[26] M.B. Barakat, M. Motlak, A.A. Elzatahry, K.A. Khalil, E.A.M. Abdelghani, Int. J. Hydrogen Energy 39 (2014) 305–316.
[27] Y. Yang, S. Li, C. Xie, et al., Chin. Chem. Lett. 30 (2019) 203–206.
[28] H. Liang, P. Hua, Y. Zhou, et al., Chin. Chem. Lett. 30 (2019) 2245–2248.
[29] F. Locatelli, J.P. Candy, B. Didillon, G.P. Niccolai, et al., J. Am. Chem. Soc. 123 (2001) 1658–1663.
[30] C. Poupin, L. Pirault-Roy, C.L. Fontaine, et al., J. Catal. 272 (2010) 315–319.
[31] I. Gandarias, J. Requies, P.L. Arias, et al., J. Catal. 290 (2012) 79–89.